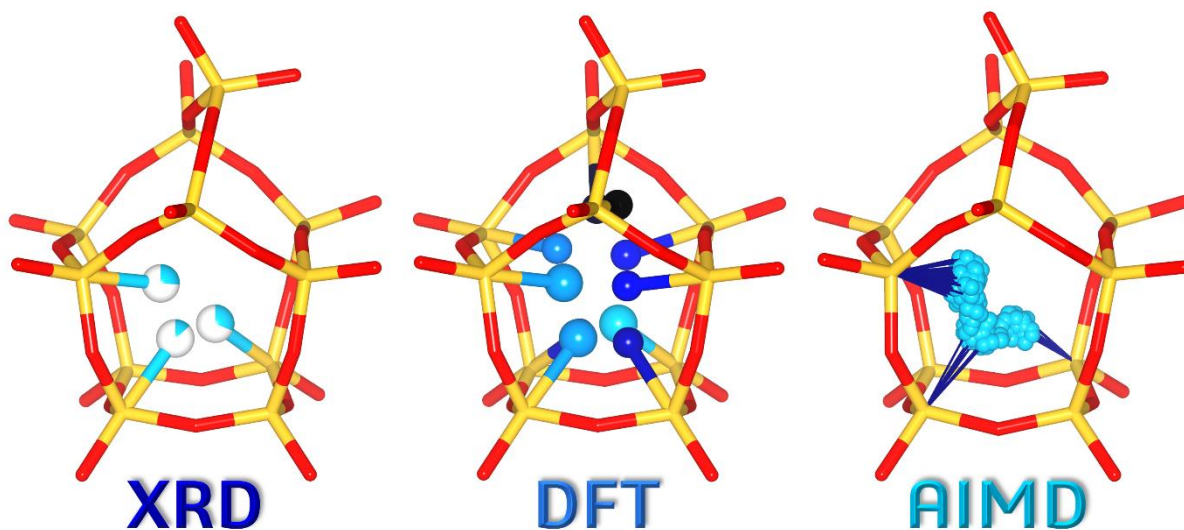# Fluoride anions in all-silica zeolites: Studying preferred fluoride sites and dynamic disorder with density functional theory calculations

Michael Fischer[1,2]

1) Faculty of Geosciences, University of Bremen, Klagenfurter Straße 2-4, 28359 Bremen, Germany

2) MAPEX Center for Materials and Processes, University of Bremen, 28359 Bremen, Germany

E-mail: michael.fischer@uni-bremen.de

Abstract

In all-silica zeolites synthesised via the "fluoride route", the fluoride anions are typically incorporated in small cages, forming $[SiO_4F]^-$ trigonal bipyramids. While diffraction and NMR experiments can elucidate the fluoride location(s) and the occurrence/absence of dynamic disorder, they provide limited insights into the factors that determine equilibrium position and dynamic behaviour. To develop a more thorough understanding, electronic structure calculations in the framework of dispersion-corrected density functional theory (DFT) were performed for five all-silica zeolites (NON, STF, IFR, STT, CHA frameworks). DFT-based predictions of the energetically preferred fluoride location within a given cage were mostly in excellent agreement with experiment. Apart from the known tendency of fluoride anions to locate close to small rings, there are no easily generalisable crystal-chemical rules to predict the most probable fluoride sites. DFT-based molecular dynamics calculations were employed to predict and explain the dynamic behaviour of the fluoride anions, which differs markedly among the different frameworks. On the basis of the simulations, it could be determined that local interactions of fluoride anions with framework Si atoms have larger impact on the (non-)occurrence of dynamic disorder than longer-range interactions with the organic structure-directing agents. In addition to providing detailed understanding of the behaviour of fluoride anions in as-synthesised all-silica zeolites, the findings of the present work could contribute to a further elucidation of the structure-directing role of fluoride during zeolite synthesis.

1 Introduction

The "fluoride route" of zeolite synthesis was pioneered by Flanigen and Patton of Union Carbide, who, in 1976, filed a patent describing the hydrothermal synthesis of sizeable single crystals of MFI-type Silicalite-1 in the presence of ammonium fluoride.[1] Subsequent research by a number of groups showed that the addition of fluoride does not only aid the preparation of large and defect-free crystals, but that it may also lead to the formation of new framework types or distinct framework compositions that are not synthetically accessible in the absence of fluoride.[2–6] The role of fluoride is particularly important in the synthesis of pure-SiO_2 (all-silica) zeolites: In these neutral-framework materials, the fluoride anions balance the charge of the cationic organic structure-directing agents (OSDAs) that are added to promote the formation of a particular structure type (while some all-silica zeolites can be synthesised in the absence of fluoride, the crystals tend to have a rather high concentration of charge-balancing defects[7,8]). Like the OSDAs, which are encapsulated in larger cages or channels, the fluoride anions are incorporated in the crystal structures of the as-synthesised zeolites, and they can be localised with diffraction methods.[9] If double four-ring (*d4r*) units are present in the structure, the fluoride anions are located at or near the centre of these cube-like cages. In structures without *d4r* cages, the fluoride anions reside in other small cages, where they are bonded to a silicon atom at one of the corners of the cage, leading to the formation of trigonal-bipyramidal $[SiO_4F]^-$ units. The first observation of such a building unit in the crystal structure of an as-synthesised all-silica zeolite was reported in 1995 for nonasil (NON framework type code[10]),[11] followed by analogous findings for various other zeolites.[12–22] The body of crystal structure data shows a preference of fluoride to bond to Si atoms that are part of small rings, most typically four-membered rings (4MRs) or, if these are not present in the structure, 5MRs.

To complement crystallographic investigations, a few authors have employed computational methods to compare different possible fluoride locations within a given zeolite: In particular, Pulido et al. carried out force-field based calculations to study the fluoride positions in all-silica zeolites with the IFR, ITH, IWR, STF, and STT topologies.[23] For those systems where experimental information was available, they observed good agreement between the computationally predicted sites and the experimental fluoride positions (as a caveat, it has to be noted that they reported their energies with a precision of only 0.1 eV = 9.6 kJ mol^{-1}, often leading to several sites having the same energy). With regard to a more general understanding of preferred fluoride sites, this comparative study yielded the following key results: In the first place, electrostatic interactions between fluoride anions and OSDA cations determine in which of the available cages the fluoride anions are incorporated. Second, the specific position within the cage is governed by localised F–Si interactions. More recently, Luo et al. employed dispersion-corrected DFT calculations to

predict the energetically preferred fluoride sites in an MWW-type all-silica zeolite.[24] They obtained very similar energies for two fluoride locations in different cages, concluding that the coexistence of two fluoride environments is responsible for the presence of two distinct resonances in the ^{19}F NMR spectrum.

The fluoride anions incorporated in $[SiO_4F]^-$ units are often disordered over two or more positions. These positions are typically related by symmetry, although there is at least one example of fluoride disorder over three non-equivalent sites in a single cage (SSZ-23, further described below).[12] Both static and dynamic disorder have been found to occur, which can be distinguished using solid-state NMR methods: If the fluoride anions are bonded to the same Si atom over extended periods of time, $i.e.$, if there is either no disorder or static disorder, the ^{29}Si NMR spectra show a sharp resonance with an isotropic chemical shift δ_{iso} of -140 to -150 ppm.[25,26] In the case of dynamic disorder, the local environment of the participating Si atoms changes between tetrahedral and trigonal-bipyramidal coordination over time, which leads to a broad ^{29}Si NMR signal in the chemical shift range of δ_{iso} = -115 to -150 ppm. NMR evidence for dynamic disorder at room temperature (RT) has been presented for ZSM-5/Silicalite-1 (MFI framework),[25,27,28] ITQ-4 (IFR),[26] and SSZ-23 (STT),[26] among other systems. The dynamic disorder can be frozen out by cooling to ~140 K,[26] and, in the case of Silicalite-1, by varying the OSDA.[27,28] The frequent occurrence of static or dynamic disorder also leads to difficulties in the accurate determination of F–Si bond distances with crystallographic methods. They tend to overestimate the bond length, typically delivering values between 1.8 and 2.0 Å.[9] More accurate distances can be obtained with NMR methods, which give F–Si distances between 1.72 and 1.79 Å.[18,29]

The dynamic behaviour of fluoride anions in all-silica zeolites and other neutral-framework zeotypes has been studied with DFT-based ab-initio molecular dynamics (AIMD) calculations in a series of recent publications.[30–32] Two of these studies focussed on zeolites and zeotypes with the AST topology, where the fluoride anions are occluded in $d4r$ cages, investigating the role of the local environment (in other words, the atomic species occupying the corners of the cage) in determining their equilibrium location and dynamic behaviour.[30,32] The third study addressed the impact of the OSDA on the dynamic disorder of fluoride anions in Silicalite-1, which contains $[SiO_4F]^-$ units.[31] It was found that the dynamic disorder is visible through distinct discontinuities ("jumps") in the time evolution of the coordinates of some fluoride anions, especially when performing AIMD simulations for temperatures above RT (373 K, 473 K). In addition, the drastic reduction of the dynamic disorder when incorporating methyl- or ethyltributylammonium instead of tetrapropylammonium cations as OSDA, previously observed in NMR experiments,[27,28] could be reproduced and rationalised on the basis of the calculations. Building upon these previous studies, the present works compares a set of five structurally different zeolites with NON,

STF, IFR, STT, and CHA topologies, which are also known to differ in the dynamic behaviour of fluoride. In the first part, DFT optimisations are employed to study the preferred fluoride locations in these zeolites, using crystal structure data of the as-synthesised forms as starting point. For each zeolite, information about the cage that hosts the fluoride anions is taken from experiment, and different positions within that cage are then compared in a systematic fashion in order to discern different factors that govern the energetically favoured fluoride position. Second, DFT-based AIMD calculations are used to study the dynamic behaviour of the fluoride anions at temperatures of 298 K, 373 K, and 473 K. In addition to evaluating whether the fluoride anions remain bonded to the same Si atom during the simulation time or "jump" between different sites, a further analysis of the role of F–Si and F-OSDA interactions is carried out. While the occurrence of dynamic disorder can be probed experimentally, the computations provide a unique possibility to better understand its origins, thereby helping to explain why fluoride anions are dynamically disordered in some zeolites, but not in others.

2 Models and methods

2.1 Choice of model systems

In order to enable a validation of the calculation results against experimental findings, the investigation largely concentrates on zeolites where crystal structure data of the as-synthesised form (*i.e.*, containing fluoride anions and OSDA cations) are available and where the dynamic behaviour of the fluoride anions has been characterised with solid-state NMR methods. These boundary conditions led to the selection of the following four systems:

- **Nonasil (NON):** The crystal structure of nonasil synthesised using cobaltocenium $[Co(cp)_2]^+$ (cp = cyclopentadienyl) cations as OSDA was reported by van de Goor et al.[11] The fluoride anions in nonasil are disordered over two symmetrically equivalent positions that are located in adjacent cages (**Figure 1**). The ^{29}Si NMR spectrum of this material shows a relatively sharp signal at a chemical shift δ_{iso} = -145 ppm at RT, indicating the presence of five-coordinated silicon atoms, and the absence of dynamic disorder.[25]

- **Mu-26 (STF):** A crystal structure refinement of STF-type zeolite Mu-26 without any disorder of fluoride anions and (6*R*,10*S*)-6,10-dimethyl-5-azonia-spiro[4.5]decane (DMASD$^+$) cations was published by Paillaud et al.[21] ^{29}Si NMR investigations of Mu-26 and of STF-type SSZ-35 show sharp doublets in the range of δ_{iso} = -145 to -148 ppm, which were explained as being due to a single $[SiO_4F]^-$ environment without dynamic disorder at RT.[21,29]
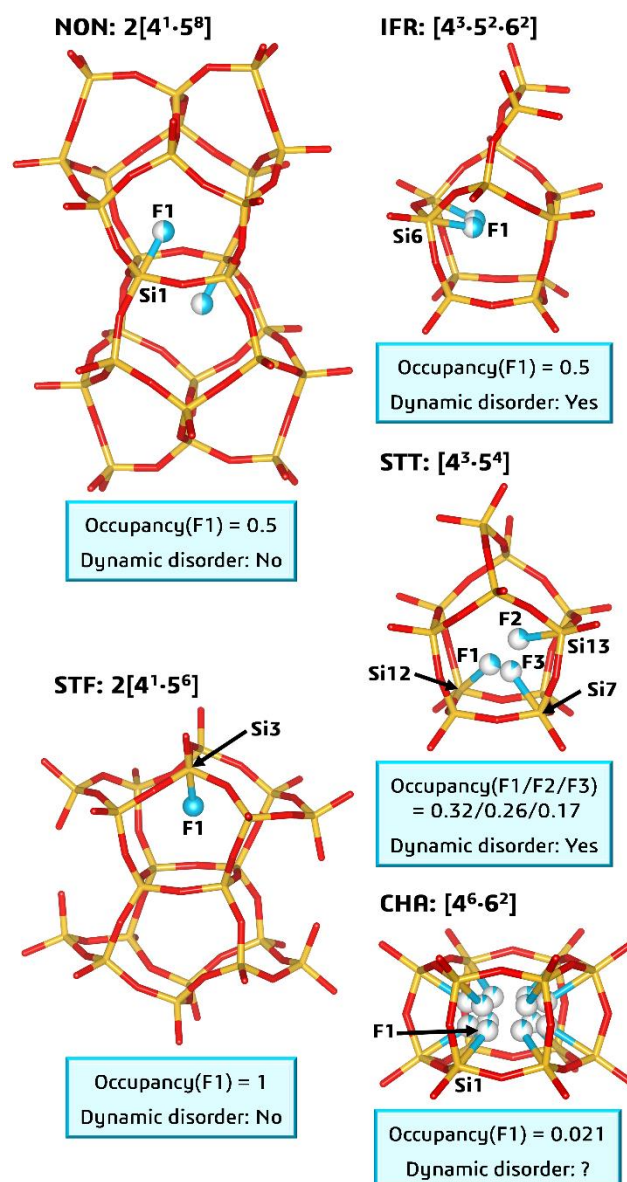
Figure 1: Visualisation of experimentally observed F positions in the five zeolites studied in the present work. In addition to the framework type code, the face symbol of the fluoride-containing cage is shown. Two fused cages are visualised for NON and STF. In this figure, the F atoms are labelled according to the original literature, whereas the remainder of this article uses a labelling scheme based on the Si atoms to which they are bonded. Colour scheme: Si = yellow, O = red, F = cyan. Fractional occupancies are shown as partially coloured atoms (for example, an atom coloured 50% cyan and 50% white corresponds to a site having an occupancy of 0.5).

- **ITQ-4 (IFR):** The structure of as-synthesised ITQ-4 was reported by Bull et al. for a sample synthesised using hydroxybenzylquinuclidinium (BQol+) as OSDA.[13,14] The fluoride anions are disordered over two symmetry-equivalent positions in the same cage (**Figure 1**). The ^{29}Si NMR spectrum of ITQ-4 recorded at T = 298 K shows a broad signal in the range of δ_{iso} = -115 to -140 ppm, which is indicative of dynamic disorder.[26]

- **SSZ-23 (STT):** The fluoride anions in as-synthesised SSZ-23 are disordered over three non-equivalent positions within the same cage (**Figure 1**).[12] NMR experiments point to a dynamic behaviour of the fluoride anions at RT, which is frozen out upon cooling to 140 K, where a sharp resonance at δ_{iso} = -142 ppm appears.[26]

Throughout this work, the zeolites will be represented by their framework type code for simplicity (for example, the label NON will be used as a short-hand for nonasil containing fluoride anions and $[Co(cp)_2]^+$ cations). It is worth emphasising that the four zeolites comprise four different types of fluoride disorder: No disorder (STF), static disorder over equivalent positions in different cages (NON), dynamic disorder over equivalent positions in the same cage (IFR), and dynamic disorder over non-equivalent positions in the same cage (STT).

In addition to the zeolites listed above, all-silica chabazite (CHA) was included as a system for which the experimental findings do not allow for definitive conclusions regarding the dynamic disorder. A crystal structure of as-synthesised Si-CHA has been reported by Villaescusa et al.[17] Despite extensive disorder of the fluoride anions, which are distributed over twelve symmetry-equivalent positions in the double six-ring cages (**Figure 1**), and evidence for F–Si bonds in the ^{19}F NMR experiments, the ^{29}Si NMR spectrum did not allow for any conclusions whether the disorder is of a static or a dynamic nature.

2.2 Preparation of zeolite models

In order to arrive at a tractable number of zeolite models with different fluoride locations, the following considerations were made: First, only positions inside those cages where fluoride is found in the experimental structures were considered (in other words, positions inside the cages shown in **Figure 1**). This reasoning follows the findings of Pulido et al., who found that the interaction with the OSDA determines in which cages the fluoride anions reside.[23] Second, vertices of a given cage were only taken into account if (at least) three of the cage edges meet at that vertex, because the formation of an $[SiO_4F]^-$ trigonal bipyramid can only be expected when the Si–F connection line points towards a face of the SiO_4 tetrahedron. Vertices where only two edges meet were not considered, because a fluoride anion that points toward the cage centre would lie on the edge of the SiO_4 tetrahedron, leading to short O–F contacts and strong repulsion. As presented for the individual zeolites in the following section, this leads to 14 distinct models for NON, 10 models for STF, IFR, and STT, and 4 models for CHA. In each case, the fluoride anions were placed at a distance of 1.85 Å from the respective Si atom in the starting structure. Furthermore, the F–Si–O angle (where O is the oxygen atom pointing away from the cage) was set to 180 degrees. For the

experimentally observed fluoride positions, the experimental positions were taken as starting point, without further adjustment of distances or angles.

The published crystal structures of IFR, STT, and CHA do not include the OSDA hydrogen atoms. In these systems, the H atoms were automatically placed using the DS Biovia *Materials Studio* software.[33] In the case of IFR, where the disorder of the OH groups leads to some unrealistic bond lengths within the OSDA molecules, the atomic coordinates of all OSDA atoms were optimised using the DREIDING force field as implemented in the *Forcite* module of *Materials Studio*.[34]

As Pulido et al. have previously studied the energetic ordering of different fluoride sites in some of the zeolites included in the present work (IFR, STF, and STT),[23] it is useful to point out the differences between their work and the approach employed here: First, Pulido et al. used empirical force field calculations, rather than dispersion-corrected DFT. Second, their models included only a single fluoride anion per unit cell, not accounting for the relatively high concentration of fluoride in real zeolites (where they are required to balance the charge of the OSDAs). Third, the calculations comparing different fluoride locations within one cage were performed for OSDA-free models, neglecting the role of F–OSDA interactions. The more recent DFT study by Luo et al. revealed rather dramatic differences between the energetic ordering obtained for zeolite models with and without OSDA cations, implying that it is necessary to include the OSDA in order to make meaningful predictions.[24]

2.3 Computational details

All calculations used the CP2K DFT code, version 7.1, as installed on the HLRN-IV facilities of the North-German Supercomputing Alliance.[35] The Perdew-Burke-Ernzerhof exchange-correlation functional[36] was used together with the pairwise D3 dispersion correction developed by Grimme and co-workers (PBE-D3),[37] in keeping with previous studies.[30–32] All calculations used a plane wave energy cutoff of 600 Ry. Only the Γ point was considered in the sampling of the first Brillouin zone. Goedecker-Teter-Hutter pseudopotentials devised by Krack were used to represent core electrons.[38] The structure optimisations made use of "molecularly optimised" (MOLOPT) Gaussian triple-zeta basis sets (TZVP for H, C, N, O, F, Si, TZVP-SR ["short range"] for Co in NON).[39] Spin-restricted calculations were performed for all systems, including the Co^{3+}-containing NON, as the cobaltocenium cation is diamagnetic. In the structure optimisations, all atomic coordinates and the unit cell parameters were optimised, fixing the symmetry of the unit cell to that of the respective crystal system. A 1×1×2 supercell was used for STF, whereas all other systems were optimised using single unit cells. Optimisations were considered converged when the following

criteria were met: Maximal geometry change = $5 \cdot 10^{-5}$ bohr, maximal residual force = $1 \cdot 10^{-6}$ Ha bohr^{-1}, maximal pressure deviation = 0.001 GPa.

The AIMD simulations employed MOLOPT Gaussian double-zeta (DZVP-SR) basis sets for all elements.[39] These calculations were performed in the *NVT* ensemble, fixing the unit cell parameters to the optimised values obtained in the structure optimisations. Single unit cells were used for NON and STT, and a 1×1×2 supercell was employed for IFR. For CHA and STF, somewhat more complex transformations were employed, which are documented in the first section of the Supporting Information (page S3 and S7). By using these supercells, there are at least four fluoride anions per simulation box (six in the case of CHA). The AIMD simulations, which were performed for temperatures of 298 K, 373 K, and 473 K, used a Nosé-Hoover thermostat with a timestep of 0.5 fs and a time constant of 50 fs.[40,41] Four separate trajectories were run for each zeolite at each temperature, with every trajectory consisting of an equilibration phase of 5,000 steps (2.5 ps) and a production phase of 15,000 steps (7.5 ps). Root mean square displacements (RMSDs) of fluoride anions as well as AIMD average structures were calculated using the VMD code, version 1.9.[42] Radial distribution functions (RDFs) of selected pairs of elements were computed with a customised code provided by Gloria Tabacchi (Università degli Studi dell'Insubria). All RDFs shown throughout this article correspond to averages over four trajectories. Structure visualisations were prepared with VESTA.[43] Sample CP2K input files, DFT-optimised structures of zeolites (in CIF format), complete AIMD trajectories (production part, in PDB format), AIMD average structures (in CIF format), and an EXCEL file containing the RDF and RMSD data have been deposited in the *Figshare* repository (https://doi.org/10.6084/m9.figshare.13603664.v1).

3 Results and Discussion

3.1 DFT optimisations: Comparison of different fluoride locations

In this section, the results of the DFT optimisations are presented individually for each zeolite, prior to discussing some more general aspects. The numerical results for all systems are tabulated in **Table S1** of the Supporting Information, and the labelling schemes of the Si atoms (which follow those used in the published crystal structures) are shown in **Figure S6**.

3.1.2 NON

In the crystal structure of as-synthesised nonasil, which has orthorhombic symmetry (space group *Pccn*), the [Co(cp)$_2$]+ cations occupying the large [5^8·6^{12}] cages are fully ordered.[11] The fluoride anions are disordered over two sites in adjacent nonasil [4^1·5^8] cages, which are fused

together via one four-membered ring. Removal of one F atom per pair of fused cages in an ordered fashion leads to a structure in space group $Pc2_1n$, which is visualised in **Figure S1**. Among different possible arrangements of fluoride anions with respect to each other, this corresponds to one of the arrangements having the highest symmetry ($Pc2_1n$ being a maximal non-isomorphic subgroup of $Pccn$[44]).

The nonasil cage has 15 vertices. 12 of these vertices correspond to meeting points of three edges, and one (Si7) to a point where four edges meet. This results in a total of 14 structures with different fluoride positions (two separate ones with F bonded to Si7) for which DFT optimisations were performed. The results of these calculations are summarised in **Figure 2**, where all fluoride positions are shown within one nonasil cage, and coloured according to their relative energy ΔE_{rel} with respect to the experimental position (the experimental position is defined as zero point of ΔE_{rel}, note that ΔE_{rel} values are always given per F atom). This position, labelled F@Si1_1, is the energetically most favourable site, with the second-best site being 5.3 kJ mol^{-1} higher in energy. All positions that are not associated with the 4MR are at least 18 kJ mol^{-1} higher in energy than the F@Si1_1 site.

3.1.3 STF

The type material of the STF framework type is the zeolite SSZ-35. The crystal structure of as-synthesised SSZ-35 was reported by Villaescusa et al.[14] In this monoclinic structure (space group $P2_1/c$), fluoride is disordered over two symmetry-equivalent positions, which are located in adjacent [4^1·5^6] cages that are fused together via the 4MR. The OSDA (racemic *N,N*-dimethyl-6-azonia-1,3,3-trimethylbicyclo(3.2.1)-octane) in this structure is heavily disordered, complicating the preparation of a starting model that is suitable for DFT calculations. Similar problems would arise for a triclinic structure (space group $P\bar{1}$) published later by Zones et al.[45] A fully ordered structure was reported by Paillaud et al., who prepared an STF-type all-silica zeolite dubbed Mu-26 using DMASD$^+$ cations.[21] In this triclinic structure (space group $P1$), only one of each pair of fused [4^1·5^6] cages contains fluoride anions, which are bonded to the Si3 atoms (**Figure 1**). The DMASD$^+$ molecules in the larger [4^4·5^8·6^6·10^2] cages are fully ordered, and their location was determined using a combination of force-field based modelling and Rietveld refinement (**Figure S2**). As this published structure does not require any modifications prior to the DFT optimisations, it was taken as starting point. Furthermore, the NMR results of Paillaud et al. confirmed the absence of a dynamic disorder of the fluoride anions, agreeing with earlier results of Fyfe et al.[29]

10 of the 12 vertices of the [4^1·5^6] cage correspond to meeting points of three edges, and DFT optimisations were carried out with fluoride anions located at these 10 sites. Four of these Si

atoms belong to the basal 4MR, four are located roughly in the equatorial plane, and another two form the apices of the cage. In the experimental structure, fluoride is bonded to one of these apical sites (F@Si3). All sites are visualised in **Figure 2**, coloured according to their relative energy with respect to F@Si3. While the second apical site F@Si4 is very close in energy to the experimental one (ΔE_{rel} = 2.4 kJ mol^{-1}), all equatorial positions are energetically unfavourable. On the other hand, one of the sites associated with the basal 4MR is energetically more favourable than the experimental position (F@Si10: ΔE_{rel} = -7.9 kJ mol^{-1}), making STF the only of the studied zeolites where the lowest-energy fluoride location deviates from the experimentally observed position. The other 4MR sites are similar in energy to F@Si3.
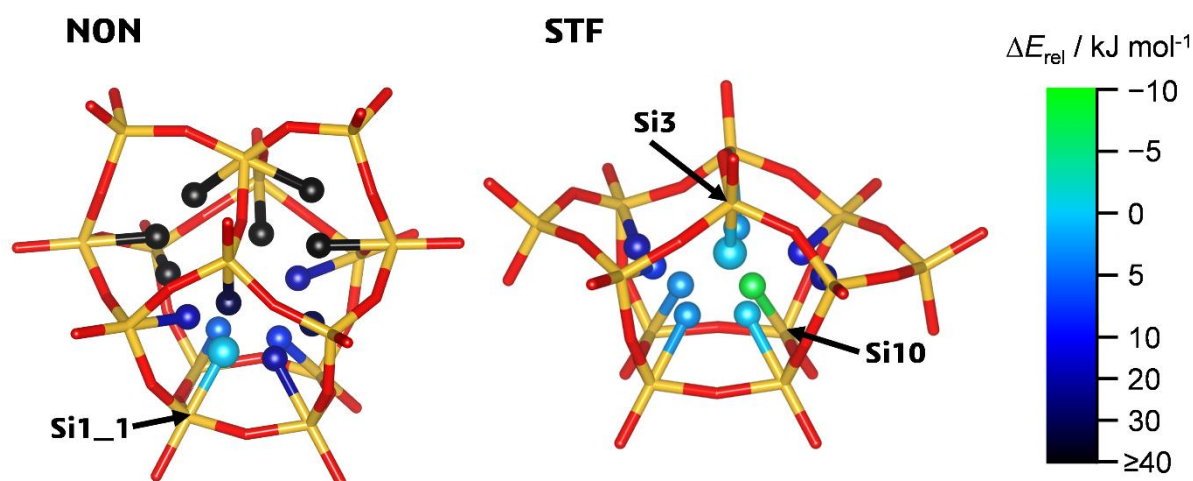

Figure 2: Energetic ordering of fluoride positions in NON and STF. All positions that were considered in separate calculations are shown within a single cage, coloured according to their relative energy. The experimentally observed sites are shown as larger spheres than other sites.

3.1.4 IFR

A crystal structure refinement of ITQ-4 including the positions of organic cations and fluoride anions was reported by Bull et al. for a sample synthesised with BQol+ as OSDA. The published structure of as-synthesised ITQ-4 is monoclinic (space group *Im*), and fluoride anions and hydroxy groups of the BQol+ cations are disordered over two positions that are related by a mirror plane (**Figure 1**).[13,14] A consideration of different possible locations of these atoms leads to six ordered structures that have *Pn*, *I*1, and *P*1 symmetries (**Figure S3**). Among these, an arrangement with *Pn* symmetry was found to have the lowest energy in preliminary DFT

optimisations, which was used as starting point for the following calculations that compared different fluoride positions.

The fluoride anions in ITQ-4 are incorporated in $[4^3 \cdot 5^2 \cdot 6^2]$ cages. While pairs of Si atoms at the corners are symmetry-related by the mirror plane in the *Im* structure, this is no longer the case in the fully ordered *Pn* structure. 10 of the 12 vertices of the cage correspond to meeting points of three edges, and all these fluoride positions were considered in the optimisations. The results are summarised in **Figure 3**. One of the experimental sites (F@Si6_1) is lowest in energy, and there is a clear energetic preference for positions associated with the four-membered rings. Interestingly, the F@Si6_2 site is 10.6 kJ mol^{-1} less favourable than the lowest-energy configuration, which is somewhat surprising in the view of the experimentally observed disorder over the two sites. The discussion will return to this point below.

3.1.5 STT

The structure of SSZ-23, the type material of the STT framework type, was reported in 1998 by Camblor et al.[12] In this structure, which has $P2_1/n$ symmetry, the *N,N,N*-trimethyl-1-adamantylammonium (TMAda$^+$) cations are incorporated in the large, unusually shaped $[4^6 \cdot 5^6 \cdot 6^5 \cdot 7^2 \cdot 9^2]$ cavities. The fluoride anions are disordered over three non-equivalent positions in the $[4^3 \cdot 5^4]$ cages, which have occupancies of 32% (F@Si12), 26% (F@Si13), and 13% (F@Si7), respectively (**Figure 1**). Apart from addition of the OSDA hydrogen atoms and removal of fluoride disorder, no further modifications were made to the experimental structure prior to the DFT calculations (**Figure S4**).

In addition to the three experimentally observed sites, there are seven other corners of the $[4^3 \cdot 5^4]$ cage to which a fluoride anion could be bonded. The DFT results for these 10 fluoride locations are summarised in **Figure 3**. Remarkably, the experimentally observed position with the highest occupancy (F@Si12) has the lowest energy, with the other two experimental sites lying within about 2.5 kJ mol^{-1}. With the exception of the F@Si6 site (ΔE_{rel} = 3.9 kJ mol^{-1}), all other configurations are at least 9 kJ mol^{-1} higher in energy. As in the cases of NON and IFR, there is a clear preference for positions associated with 4MRs, but not all of these positions are energetically favourable.
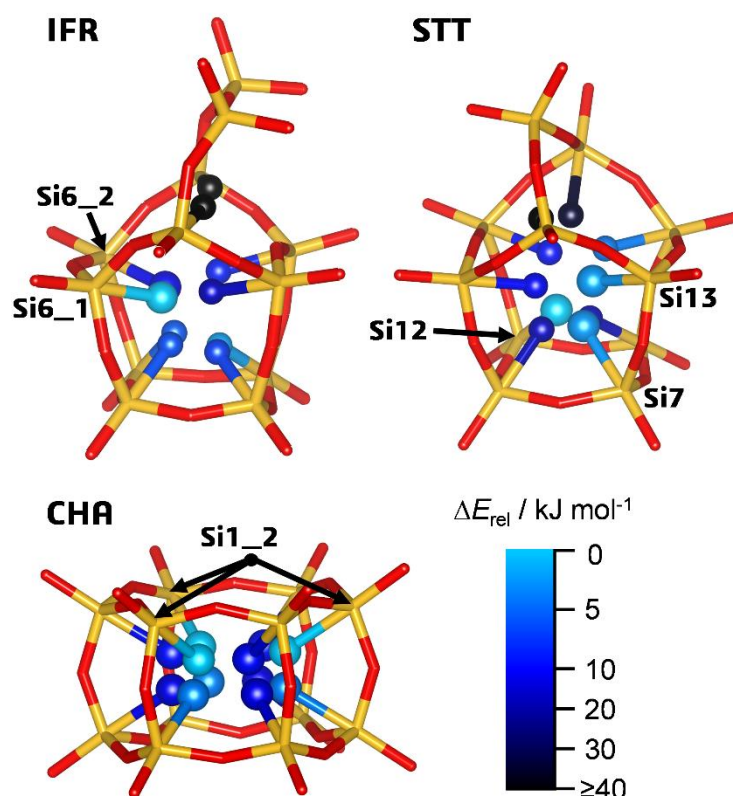
Figure 3: Energetic ordering of fluoride positions in IFR, STT, and CHA, with individual sites coloured according to their relative energy. Experimentally observed sites are shown as larger spheres. All 12 positions are shown in the *d6r* cage of CHA, although there are only 4 non-equivalent fluoride sites.

3.1.6 CHA

The crystal structure of the zeolite mineral chabazite has been known since the 1950s,[46] and that of calcined all-silica CHA was reported in 1998.[47] A structure refinement of as-synthesised Si-CHA containing TMAda+ cations and fluoride anions was published in 2003 by Villaescusa et al.[17] In this structure, which has the rhombohedral $R\bar{3}m$ symmetry of the CHA aristotype, the fluoride anions are twelve-fold disordered in the double six-ring (*d6r*) cages (face symbol [$4^6 \cdot 6^2$]), and the TMAda+ cations, which occupy the larger *cha* ([$4^{12} \cdot 6^2 \cdot 8^6$]) cages, exhibit significant orientational disorder (**Figure S5**). The first step in the preparation of the structure for the DFT calculations consisted in a removal of the OSDA disorder, and addition of hydrogen atoms, leading to a structure in space group *R*3. This structure contains four non-equivalent fluoride sites, each having three symmetry images per *d6r* cage (**Figure S5**). A further symmetry reduction to space group $P3_2$ is necessary in order to reduce the number of fluoride anions per *d6r* cage to one (balancing the charge of one TMAda+ cation per *cha* cage).

The four resulting fluoride positions, labelled F@Si1_1 to F@Si1_4, were considered in the DFT calculations. Despite the identical local environment, the energy difference between the lowest-energy site (F@Si1_2) and the least favourable position is far from insignificant, amounting to 12.3 kJ mol^{-1} (**Figure 3**). It is noteworthy that pairs of sites where the Si atoms are at opposite ends of the same equatorial Si-O-Si linkage are relatively close in energy, a point that will be elaborated in the following subsection.

3.1.7 General features of preferred fluoride sites

In all five zeolites, the fluoride position with the lowest energy is associated with a four-membered ring. This result agrees with most experimental crystal structures (with the exception of STF, discussed above) and with the previous force field study of Pulido et al., who also observed a preference for positions at 4MRs.[23] In fact, it has been recognised that fluoride anions exert a structure-directing effect favouring structures having a high density of 4MRs, as they tend to stabilise these rings.[3] Beyond this, however, there are no clearly identifiable trends in the energetic ordering of different sites. For example, the preference for 4MRs might give rise to the assumption that positions at a vertex where two 4MRs meet should be particularly preferred. While this is true for the F@Si12 site in STT, neither of the four positions in IFR that are associated with the basal 4MR, which shares two edges with other 4MRs, are lower in energy than the F@Si6_1 site. Furthermore, one might expect that "similar" building units also show a similar energetic ordering. This is, to a degree, true for the [$4^1 \cdot 5^8$] cage in NON and the [$4^1 \cdot 5^6$] cage in STF, which are characterised by a basal 4MR surrounded by four 5MRs. In both zeolites, one of the four 4MR sites is distinctly favoured over the other three sites. A different picture emerges when comparing IFR and STT: Despite the similarity of the [$4^3 \cdot 5^2 \cdot 6^2$] and [$4^3 \cdot 5^4$] cages, both of which have a basal 4MR that is surrounded by two 4MRs and two 5MRs, the energetic ordering of corresponding fluoride positions is fairly different (**Figure 3**).

CHA is particularly interesting in this regard, as there is only one type of T site in the CHA framework. Since the local environment is identical for all four configurations considered, other explanations must be developed to rationalise the observed range of ΔE_{rel} values. In the first instance, one might envisage some relationship to certain interatomic distances between fluoride anions and OSDA atoms. For example, it would be reasonable to expect an inverse correlation between DFT energy and the distance from the fluoride anion to the positively polarised TMAda$^+$ nitrogen atom. However, an analysis of the three shortest F–N, F–C, and F–H distances in the optimised structures of CHA, compiled in **Table S2**, reveals no discernible correlation with the sequence of ΔE_{rel} values. As pointed out above, the two more favourable fluoride sites (F@Si1_2

and F@Si1_4) are associated with Si atoms at opposite ends of one equatorial Si–O–Si linkage (equatorial = the oxygen atom is part of the central plane of the *d6r* unit), and the less favourable sites are associated with the other equatorial linkage. A visualisation of the respective structures in a projection along the *c* axis reveals that these equatorial linkages differ in their proximity to the screw axis, leading to shorter F–F distances of about 7.3 Å for F@Si1_1 and F@Si1_3 compared to ~8.4 Å for F@Si1_2 and F@Si1_4 (**Figure S7**). While these distances are too long to expect any significant fluoride-fluoride repulsion, the number of Si–O–Si linkages between neighbouring [SiO$_4$F]$^-$ trigonal bipyramids differs markedly: In the former, energetically unfavourable case, there are only two such linkages between adjacent [SiO$_4$F]$^-$ units, compared to four for the latter case. It seems plausible to conclude that the local distortions that occur as a consequence of the formation of [SiO$_4$F]$^-$ trigonal bipyramids can be accommodated more easily when these units are distributed rather evenly in the structure, leading to a lower energy for the F@Si1_2 and F@Si1_4 structures. While one would not expect such a strict ordering of fluoride anions in real Si-CHA samples, it points to a tendency to maximise F–F distances between fluoride anions located in adjacent *d6r* units. Although this appears to be the main factor determining the energetic ordering of the models considered, it is worth noting that that there is also an energy difference of about 3 to 4 kJ mol^{-1} between sites associated with the same equatorial Si–O–Si linkage. This difference can indeed be attributed to attractive interactions with the OSDA molecules, as the F–N distances are shorter for the sites in the "upper" part of the *d6r* cage (F@Si1_1 and F@Si1_2).

As a second example, the energetic ordering of those fluoride sites that are associated with 4MRs in IFR is investigated. Since the shortest F–F distance corresponds to the length of the *c* axis for symmetry reasons, it is essentially identical for all configurations, and the observed energy differences cannot be explained on this basis. An evaluation of distance between fluoride anions and N atoms of the closest BQol$^+$ cation, tabulated in **Figure 4**, shows that this distance is shortest for the lowest-energy site (F@Si6_1), indicating that attractive interactions between the positively polarised part of the OSDA and the fluoride anions play an important role in determining the energetically most favourable location. However, the large difference of 10.6 kJ mol^{-1} between the F@Si6_1 and F@Si6_2 sites, for which the F–N distance is (virtually) identical, cannot be rationalised on this basis. This observation can be explained with repulsive interactions between the fluoride anions and the O atoms of the BQol$^+$ OH group, both of which bear a significant negative charge (according to Hirshfeld partitioning,[48] q_{Hsf}(F) = -0.49 e and q(O$_{BQol}$) = -0.75 e). As the distance between these negatively polarised sites is significantly shorter for F@Si6_2 (**Figure 4**), a larger electrostatic repulsion arises. Finally, the low energy of the F@Si1_2 position is noteworthy. Here, one of the surrounding oxygen atoms acts as hydrogen bond acceptor for the O–H···O bond from the BQol$^+$ OH group. Presumably, this hydrogen bond leads to a perturbation in the environment of the Si1_2 atom that facilitates the formation of an [SiO$_4$F]$^-$ trigonal pyramid.

IFR

	ΔE_{rel} [kJ mol^{-1}]	d(F–N) [Å]
F@Si6_1	0	5.99
F@Si6_2	10.6	6.00
F@Si1_1	7.4	7.13
F@Si1_2	2.0	7.15
F@Si2_1	17.3	6.81
F@Si2_2	8.9	7.03
F@Si3_1	6.5	6.30
F@Si3_2	6.0	6.39

F@Si6_1 d(F–O$_{BQol}$) = 5.80 Å

F@Si6_2 d(F–O$_{BQol}$) = 5.45 Å
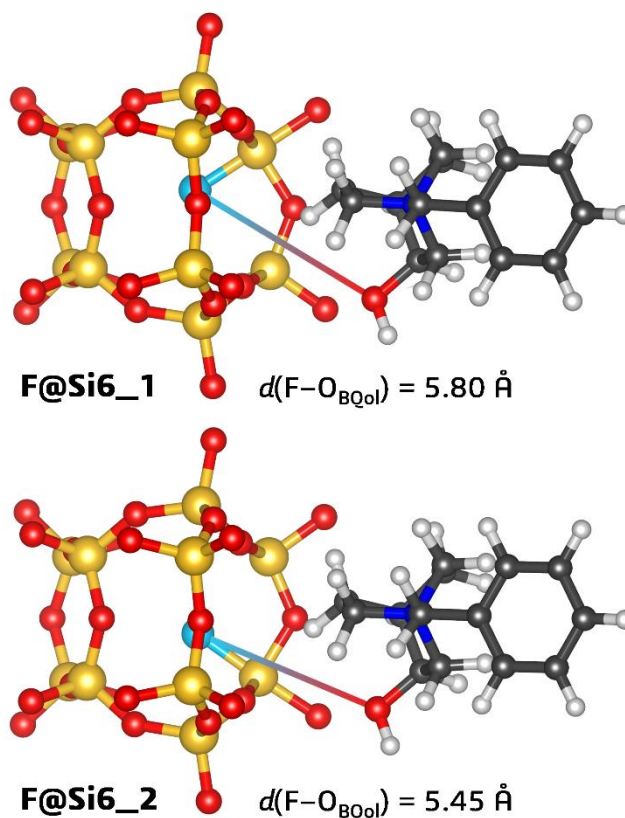
Figure 4: Left: Table summarising ΔE_{rel} values and F–N distances for different fluoride positions in IFR (excluding the F@Si8 positions, which are much higher in energy [**Figure 3**]). **Right:** Visualisation of the relative arrangement of fluoride anions and O$_{BQol}$ atoms in the F@Si6_1 and F@Si6_2 cases.

It has to be conceded that the explanations invoked for CHA and IFR are specific to the respective framework-OSDA combinations and cannot be generalised. For example, none of the arguments developed above can explain the variation in energy among the four 4MR sites in NON, which are topologically equivalent (*i.e.*, they are equivalent by symmetry in the NON aristotype, but the incorporation of fluoride and OSDA in a fully ordered fashion renders them inequivalent in the $Pc2_1n$ structure): Although F–F distances vary, the most favourable F@Si1_1 case is not the configuration with the longest distances (moreover, the fluoride sites are far apart in comparison to CHA, with all F–F distances above 9 Å). With regard to framework-OSDA interactions, one of the oxygen atoms of the [SiO$_4$F]$^-$ unit acts as acceptor of a weak C–H···O hydrogen bond (with H···O distances of 2.4 to 2.5 Å) in three of the four models, which, however, differ by up to 20 kJ mol^{-1}. These observations underline that it is challenging to discern the individual factors determining the energetically preferred fluoride location in a given system, as there are few generalisable rules.

3.1.8 Unit cell parameters and F–Si distances

Prior to discussing the results of the AIMD simulations, it is worthwhile to compare optimised unit cell parameters and F–Si distances to the experimental values. As is visible in **Table 1**, the lattice parameters consistently agree with experimental values to within 1%, although a certain systematic tendency to overestimate the unit cell dimensions can be identified. The good performance of the PBE-D3 functional in reproducing experimental lattice parameters of as-synthesised zeolites agrees with the results of a previous benchmarking study including various guest-free (calcined) zeolites and zeotypes.[49]

Table 1: Experimental and DFT-optimised unit cell parameters and F–Si distances. For STF, both the experimental fluoride position F@Si3 and the lowest energy configuration F@Si10 are included. Relative errors in unit cell parameters are given in brackets.

	a / Å	b / Å	c / Å	α / °	β / °	γ / °	d(F–Si) / Å
NON, exp[11]	22.125	13.612	14.889	90	90	90	1.84
NON, DFT (F@Si1_1)	22.211 (+0.39%)	13.656 (+0.32%)	14.893 (+0.03%)	90	90	90	1.76
STF, exp[21]	11.321	11.433	7.403	96.43	94.31	104.63	1.90 (XRD) 1.72-1.79 (NMR)[29]
STF, DFT (F@Si3)*	11.360 (+0.35%)	11.500 (+0.58%)	14.842 (+0.25%)	96.23 (-0.21%)	94.15 (-0.17%)	104.64 (+0.01%)	1.77
STF, DFT (F@Si10)*	11.372 (+0.45%)	11.528 (+0.83%)	14.693 (-0.76%)	95.64 (-0.82%)	94.50 (+0.19%)	105.20 (+0.54%)	1.77
IFR, exp[13,14]	18.571	13.494	7.715	90	102.30	90	1.92
IFR, DFT (F@Si6_1)	18.577 (+0.03%)	13.584 (+0.66%)	7.770 (+0.71%)	90	101.86 (-0.43%)	90	1.79
STT, exp[12]	12.960	21.792	13.598	90	101.86	90	1.94
STT, DFT (F@Si12)	13.082 (+0.95%)	21.960 (+0.77%)	13.643 (+0.33%)	90	101.17 (-0.67%)	90	1.81
CHA, exp[17]	13.490	13.490	14.758	90	90	120	2.00
CHA, DFT (F@Si1_2)	13.570 (+0.59%)	= a	14.891 (+0.90%)	90	90	120	1.79

* Optimised in a 1×1×2 supercell

With regard to the F–Si distances, the experimental values obtained with diffraction methods vary considerably, ranging from 1.84 Å for NON to 2.00 Å for CHA. It is well-known that the occurrence of fluoride disorder causes the apparent F–Si distances determined in XRD structure refinements to be longer than the actual distances, because the local environment that is probed by diffraction corresponds to an average over two different environments, SiO_4 tetrahedra and $[SiO_4F]^-$ trigonal

bipyramids.[9,29] It has to be noted that this argument does not explain the experimental F–Si distance of 1.90 Å in STF, where the fluoride anions are not disordered. As solid-state NMR methods probe the local environment, they can give more realistic F–Si bond lengths, provided that there is no dynamic disorder. For STF, NMR experiments delivered an F–Si distance of 1.72 to 1.79 Å,[29] and values of 1.74/1.79 Å were obtained for SFF-type SSZ-44, where the XRD value amounts to 1.89 Å (the reported variation of NMR-derived distances for a given system arises from the application of more than one measuring method in the respective studies).[18] The DFT optimisations deliver F–Si distances that agree very well with these values, ranging from 1.76 to 1.81 Å. Given the essentially identical bonding environment, the variation among different zeolites is non-negligible, with the shortest distance being found in NON, and the longest one in STT, a point that will be considered when discussing the dynamic behaviour. It is worth noting that F–Si distances between 1.71 and 1.78 Å were reported in earlier DFT studies of all-silica zeolites containing $[SiO_4F]^-$ units.[22,31,50]

3.2 AIMD simulations: Dynamic disorder of fluoride anions

3.2.1 Occurrence of dynamic events

For NON, IFR, STT, and CHA, the AIMD simulations were performed for zeolite models with fluoride in the energetically preferred location as determined in **3.1**, whereas both the F@Si3 (experimental) and F@Si10 (lowest-energy) cases were considered for STF. In a first step, the RMSDs of individual fluoride anions and the F–Si distances in the AIMD average structures were evaluated. They are tabulated in the third section of the Supporting Information. Following the same approach as in the previous study on Silicalite-1,[31] unusually large RMSD(F) values (for the respective temperature) in combination with elongated F–Si distances were employed as reliable indicators for the occurrence of one or several dynamic events during the 7.5 ps covered by each AIMD trajectory. In order to determine the actual number of dynamic events N(DE), the evolution of the atomic coordinates over time was plotted for these fluoride anions. A dynamic event was then identified as a sudden "jump" in one (or more) coordinates. **Figure 5** contrasts the evolution of the y coordinate of a fluoride anion in IFR that undergoes a dynamic event with that of another anion that remains bonded to the same Si atom during the whole 7.5 ps (both examples were taken from the same trajectory). **Table 2** lists the total number of dynamic events within 30 ps (four 7.5 ps trajectories).
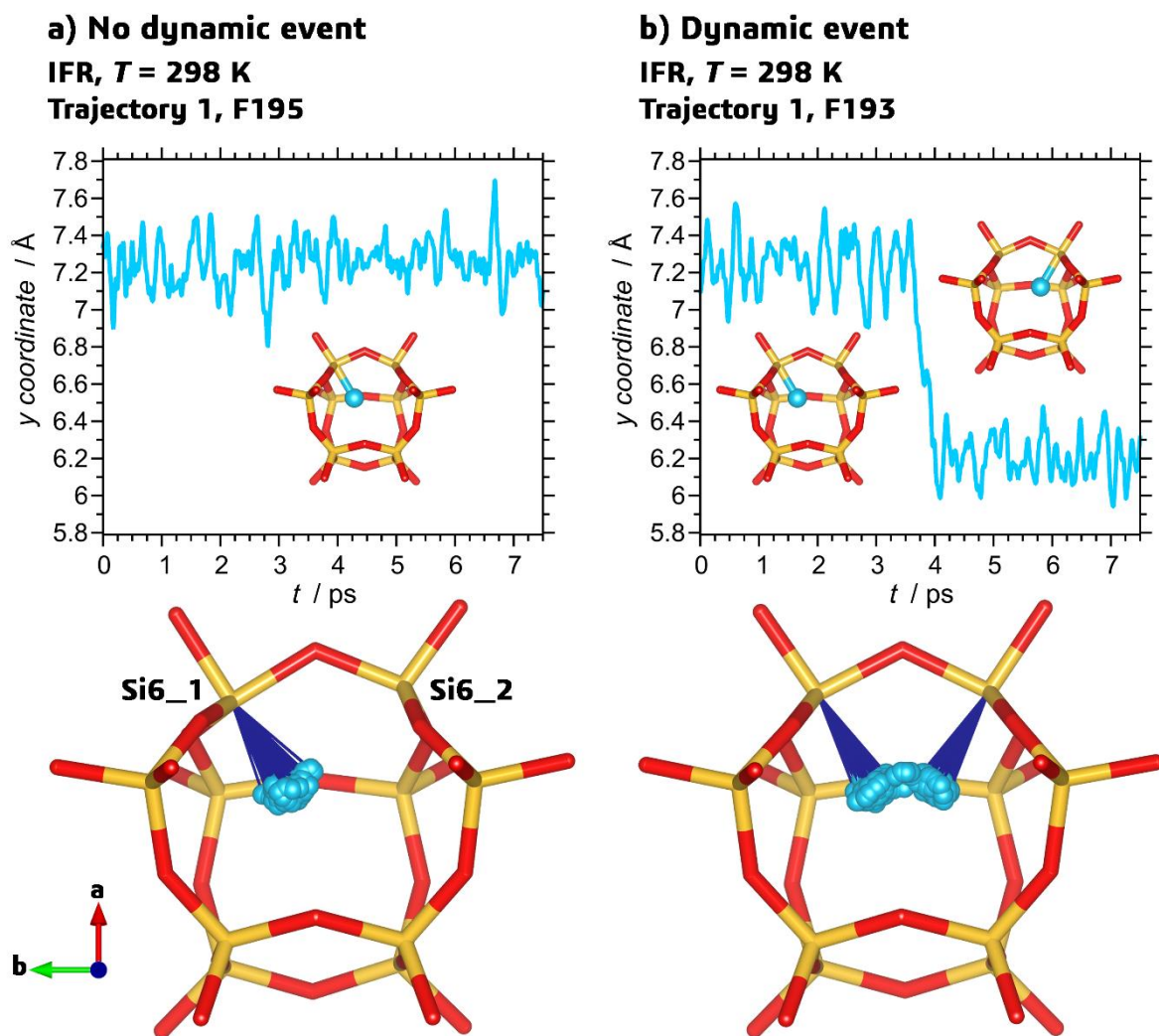
Figure 5: Top: Time evolution of the *y* coordinate of two different fluoride anions in IFR at 298 K. While the fluoride anion shown in a) remains bonded to the same Si atom, the one shown in b) undergoes a dynamic event after about 4 ps. **Bottom:** Visualisation of the trajectory of these fluoride anions within the cage. The positions of Si and O atoms are taken from the average structure. Two Si atoms and a bridging O atom are removed from the cage visualisation to improve the visibility of the fluoride trajectory. Thin blue lines mark F–Si contacts ≤ 1.9 Å. The labels "F193" and "F195" correspond to the numbers of the respective atoms in the AIMD input files and output trajectories.

Table 2: Number of dynamic events N(DE) obtained for different temperatures and relative energies for secondary fluoride locations (= location after the dynamic event).

	Exp. dynamic disorder?	N(DE) 298 K	N(DE) 373 K	N(DE) 473 K	ΔE_{rel} (F$_{2nd}$) / kJ mol^{-1}
NON	NO	0	0	0	5.4 (F@Si2_2)*
STF, F@Si3	NO	0	2	6	2.4 (F@Si4)
STF, F@Si10	NO	0	1	2	8.1 (F@Si1)
IFR	YES	5	5	13	10.6 (F@Si6_2)
STT	YES	1	3	11	2.6 (F@Si7), 2.5 (F@Si13)
CHA	?	0	2	4	9.6 (F@Si1_1), 3.8 (F@Si1_4)

* In the absence of any dynamic event, the second-lowest energy position was included for NON.

If only a temperature of 298 K is considered, the AIMD results are in perfect qualitative agreement with experiment for the four zeolites for which NMR measurements could elucidate the dynamic behaviour: While no dynamic events are observed in NON and either of the STF systems, dynamic disorder of fluoride anions does occur in IFR and STT. At 373 K, however, the picture is less clear cut for STF and STT, as they differ only by one or two dynamic events (depending on the fluoride location in STF). When moving to 473 K, the qualitative difference is restored, with roughly twice as many dynamic events in STT compared to STF. In the view of the limited duration of the simulations, it is clear that these results have to be interpreted with caution, as the total number of dynamic events is small and statistical uncertainties are large. On a qualitative level, however, it seems reasonable to distinguish the behaviour of the four zeolites as follows: (1) In NON, dynamic disorder of the fluoride anions can be ruled out up to relatively high temperatures. (2) In STF, there is no evidence for dynamic disorder at RT, but it seems reasonable to expect its occurrence at elevated temperatures. The fluoride location has only a modest effect on the dynamic behaviour. (3) While room-temperature dynamic disorder in STT appears likely, a longer simulation time would be necessary to substantiate this conclusion if no experimental results were available. (4) IFR exhibits pronounced dynamic disorder at all temperatures.

With no dynamic events at RT and 2/4 events at 373/473 K, the results for CHA are most similar to those of STF, indicating that the observed disorder of fluoride anions over 12 positions in the *d6r* cage is of a static nature at room temperature. This agrees with the absence of any broad signal in the range of δ_{iso} = -115 to -150 ppm in the ^{29}Si NMR spectrum.[17] Given the prominent disorder in the crystal structure, with many fluoride sites in relatively close proximity, the lack of evidence for dynamic disorder appears somewhat surprising. However, these observations highlight that the time-averaged crystal structure alone allows for no reliable conclusions regarding the dynamic behaviour. This is especially true for sites with low occupancy, where the atomic displacement parameters refined from diffraction data must be regarded with caution.

3.2.2 System-by-system analysis of fluoride motion

Following the initial analysis of the occurrence/absence of dynamic disorder and its dependence on temperature, it is insightful to take a closer look at the fluoride displacements associated with the individual dynamic events. To this end, both the average positions and the evolution of the atomic coordinates over time were analysed for those anions that undergo dynamic events. For the representative cases that are discussed in the following, a visualisation of the fluoride trajectory plotted into the average structure of the surrounding cage is presented. Additionally, the fourth section of the Supporting Information contains plots of the time-averaged fluoride locations as well as the evolution of the relevant atomic coordinates.

This analysis is most straightforward for IFR: All dynamic events in this zeolite are associated with a prominent jump in the y coordinate of the respective fluoride anion, which changes by about ~1 Å. This is visualised exemplarily in **Figure 5b**, all other dynamic events show a qualitatively similar behaviour. There are some cases where more than one jump of a single fluoride anion occurs over the course of 7.5 ps. The fluoride trajectory, also visualised in **Figure 5b**, shows that this movement along the b direction corresponds to a jump between the F@Si6_1 and F@Si6_2 sites, in agreement with the experimentally observed disorder (**Figure 1**). It is interesting to note that this disorder occurs despite the rather large energy difference of 10.6 kJ mol^{-1} obtained in the DFT optimisations (**Figure 4**). This point will be revisited below, when discussing the role of OSDA dynamics. **Figure 5b** also shows that, rather than moving along a straight line between the two sites, the fluoride anion follows an arc-like trajectory, thereby maintaining shorter contacts to the framework.

In the STF, F@Si3 structure, the dynamic events are primarily associated with a change of the x coordinate (**Figure 6**). This corresponds to a jump between the F@Si3 site and the other apical site, F@Si4, with the fluoride anion following an arc-like trajectory as observed above for IFR. The mobility between these two sites is not surprising in the view of the DFT optimisation results, as they are spatially and energetically close together. In the STF, F@Si10 case, the dynamic events also coincide with displacements along the a direction, corresponding to a mobility between the F@Si10 and F@Si1 sites. According to the DFT optimisations, the energy difference between these two sites amounts to about 8 kJ mol^{-1}. In the light of this sizeable energy difference, it seems plausible to expect that dynamic events occur only at elevated temperatures, where the thermal energy is sufficient to overcome the energetic barrier.
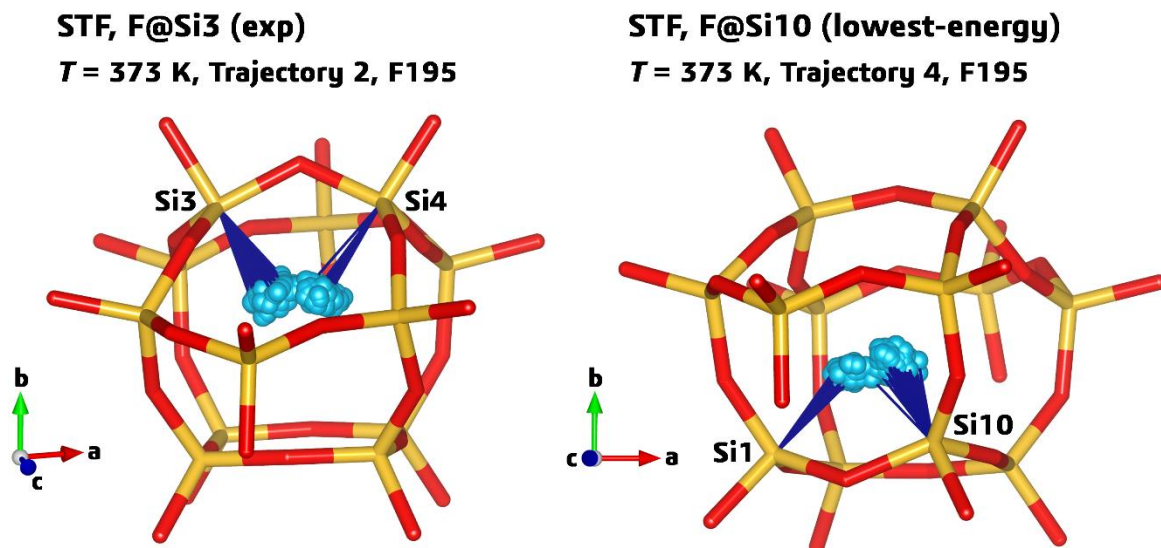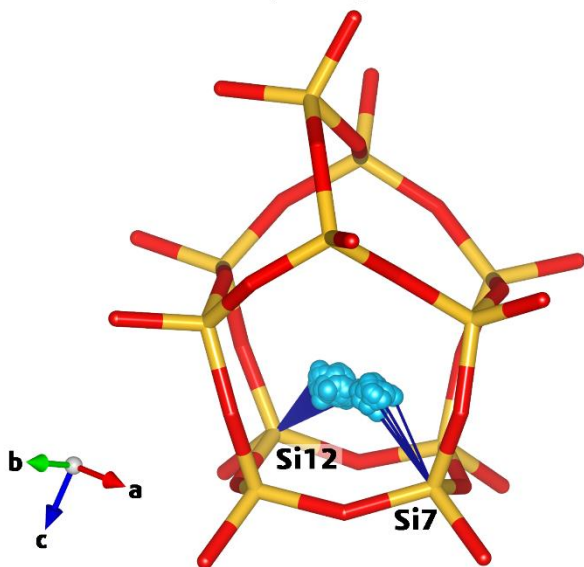
Figure 6: Representative individual trajectories of fluoride anions undergoing dynamic events in STF, F@Si3 (left) and STF, F@Si10 (right). Thin blue lines mark F–Si contacts ≤ 1.9 Å.

The most complex situation is found in the STT zeolite, where qualitatively different changes in the atomic coordinates occur during different dynamic events. Four representative examples are compiled in **Figure 7**. In the first case (**Figure 7a**), the fluoride anion moves diagonally across the 4MR, from the F@Si12 site (the initial position) to the F@Si7 site, another one of the three experimentally observed fluoride locations. **Figure 7b** actually shows two consecutive events, with fluoride again moving from F@Si12 to F@Si7, but with a transient location at F@Si4. The bonding of fluoride to the Si4 atom is short-lived, lasting only for about 1 ps. The apparent instability of this fluoride location can be explained straightforwardly with its much higher energy (ΔE_{rel} = 18.4 kJ mol^{-1}). In the scenario depicted in **Figure 7c**, the fluoride anion is located at the F@Si7 site at the beginning, so it must have moved to this position during the equilibration phase. The dynamic event occurring during the production phase corresponds to a jump to the F@Si13 site, the third experimentally observed site. The last example, shown in **Figure 7d**, corresponds to a series of two dynamic events that involves all three experimental positions (F@Si12 ➜ F@Si7 ➜ F@Si13). It is intriguing to see that the experimentally observed disorder over these three sites is fully reproduced in the AIMD simulations, with no other site being occupied (except for the short-lived occupation of the F@Si4 site). Given the relatively short simulation time, and the fact that only the F@Si12 position is occupied in the starting structure, the simulations cannot give any quantitative information about the relative occupancy of different sites. However, based on the excellent qualitative agreement with experiment, one could envisage such quantitative predictions by means of AIMD simulations covering a longer time.
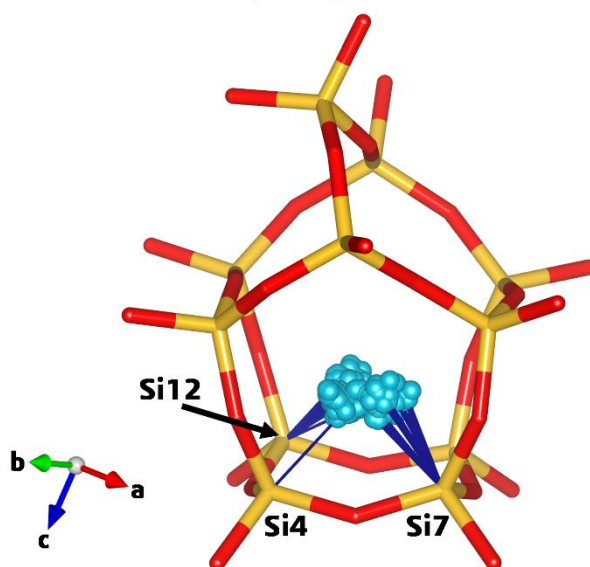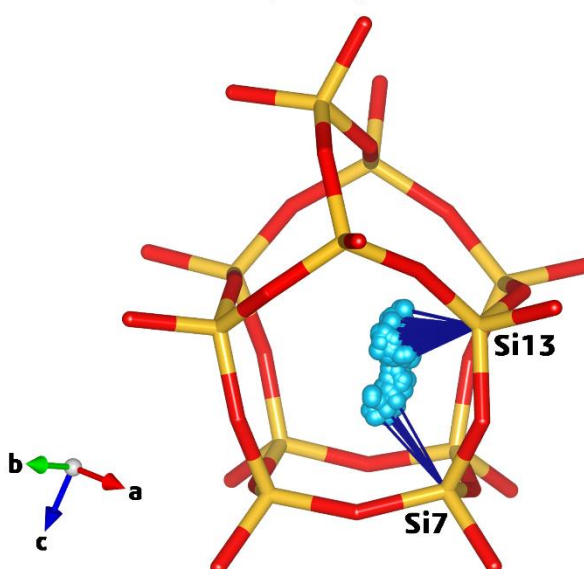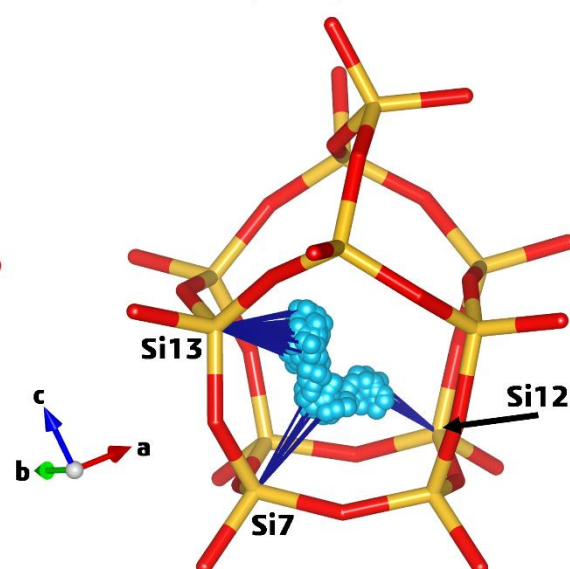
Figure 7: Representative individual trajectories of fluoride anions undergoing dynamic events in STT. Thin blue lines mark F–Si contacts ≤ 1.9 Å.

Finally, two different types of dynamic events occur in CHA. The first type, shown in **Figure 8a**, is associated with a movement within the *ab* plane, corresponding to a movement from the F@Si1_2 site to a neighbouring F@Si1_1 site. Despite the rather large energy difference of 9.6 kJ mol^{-1} obtained in the optimisations, the fluoride anion seems to be relatively stable at the F@Si1_1 site. An altogether different behaviour is observed for the other type of dynamic event (**Figure 8b**):

Here, the fluoride anion moves along the *c* direction towards the F@Si1_4 site, but returns more or less immediately to its initial position, with the residence time at the F@Si1_4 site remaining below 1 ps. It might be debatable whether such short-lived displacements from the equilibrium position should be counted as dynamic events at all. However, they were included in the analysis as the present work aims to capture as much of the dynamic behaviour as possible.
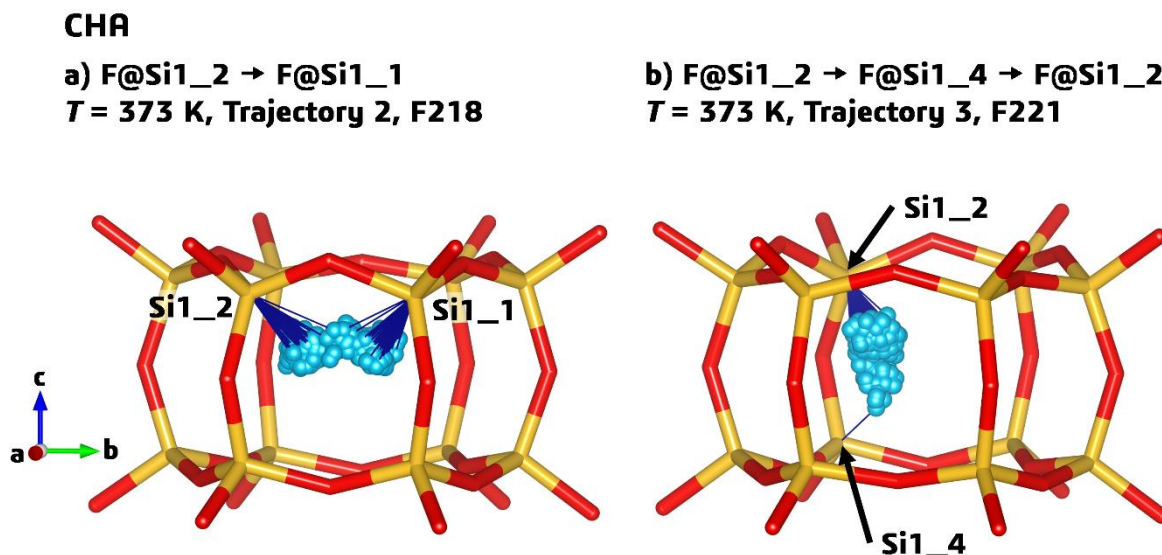

Figure 8: Representative individual trajectories of fluoride anions undergoing dynamic events in CHA. Thin blue lines mark F–Si contacts ≤ 1.9 Å.

3.2.3 The role of F–Si interactions

The previous subsection has already shown that there is no one-to-one correspondence between the energetic ordering of fluoride sites obtained from the DFT optimisations and the occurrence of dynamic disorder in the AIMD simulations: There are some cases where the observations can be understood on the basis of the optimisation results, because the primary (initial) fluoride location and the secondary site at which fluoride resides after the dynamic event are both spatially close together and close in energy, *i.e.*, the value of ΔE_{rel} obtained for the secondary fluoride position is small. However, this is not always the case, as highlighted for IFR and CHA. The compilation of ΔE_{rel} values in **Table 2** emphasises that the results of the DFT optimisations alone would not allow for reliable predictions regarding the (non-)occurrence of dynamic events, clarifying that the atomic motion at finite temperature needs to be considered explicitly.

Figure 9 compares the F–Si RDFs calculated from the AIMD trajectories at 298 K. The first maximum, which corresponds to the primary F–Si bond, is centred at 1.76±0.01 Å for all zeolites except STT, where it is shifted to about 1.8 Å. Moreover, the maximum is somewhat broader for IFR, STT, and CHA compared to NON and the two STF models. In the distance range between the first and second maximum, non-zero $g(r)$ values are prominently visible for IFR and STT (see inset of **Figure 9**). These F–Si distances between about 2.0 and 2.2 Å occur during the dynamic events, when a fluoride anion moves between primary and secondary Si atom. Accordingly, the RDF drops (exactly or almost) to zero for the other zeolites, where no dynamic events occur at this temperature. The most noteworthy difference in the F–Si RDFs, however, is the onset of the second maximum: The rise in $g(r)$, for the present purpose arbitrarily defined using the F–Si distance where $g(r)$ exceeds 0.1, begins at about 2.25 Å for IFR and STT, at ~2.3 Å for CHA, at 2.35 to 2.4 Å for STF, depending on fluoride location, and at ~2.5 Å for NON. It is striking to observe that this sequence shows a direct correspondence with the dynamic behaviour: Those zeolites where the second maximum begins at the shortest F–Si distances exhibit RT dynamic disorder (IFR, STT), whereas the only system showing no dynamic disorder at any temperature, NON, has by far the largest separation between the first and second maximum. STF and CHA, for which dynamic disorder is predicted for elevated temperatures, fall between the two extremes. The F–Si RDFs obtained at 373 K and 473 K (**Figures S12** and **S13**) show a qualitatively analogous behaviour, with the most notable difference being the increase of the $g(r)$ values between the first and second maximum that stems from the increased number of dynamic events. Altogether, it can be concluded that the local environment of a fluoride anion, specifically the distance from its initial location to secondary Si sites, determines its ability to move between different Si atoms. The energetic ordering of different locations in the static structure appears to play a less important role, presumably because the thermal motion tends to reduce the energy differences between different fluoride locations.

A last aspect that is worth mentioning with regard to F–Si interactions is the relatively large range of F–Si bond lengths in the DFT-optimised structures: The shortest distance of 1.76 Å is calculated for NON, whereas distances of 1.81/1.79/1.79 Å, respectively, are found for STT/IFR/CHA. In the view of the findings discussed above, the slight expansion of the F–Si distances in these systems can be attributed to attractive interactions with secondary Si atoms. This interaction weakens the F–Si bonds, thus rendering the fluoride anions more susceptible towards a displacement from their equilibrium location and making dynamic disorder more likely.
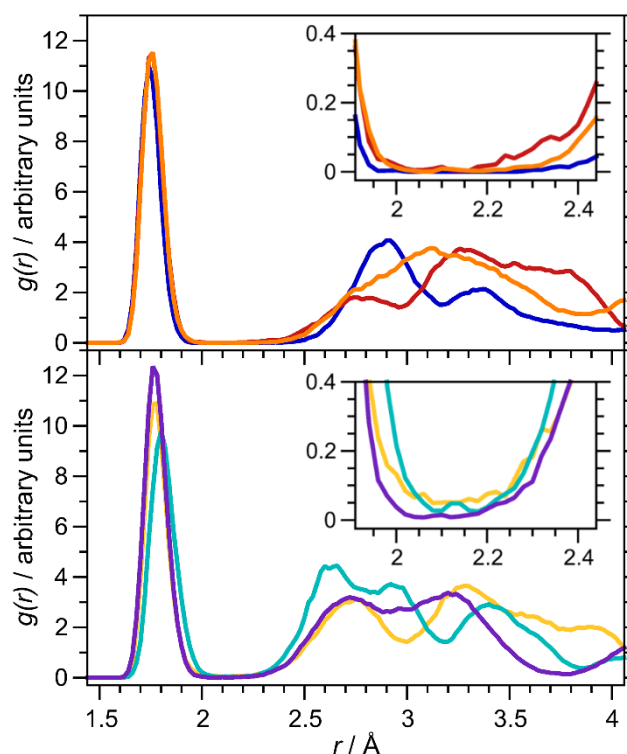
Figure 9: F–Si RDFs obtained from 298 K trajectories. **Top:** NON (blue), STF, F@Si3 (dark red), STF, F@Si10 (orange). **Bottom:** IFR (yellow), STT (cyan), CHA (purple).

3.2.4 The role of F–OSDA interactions

Previous NMR studies of MFI-type Silicalite-1 revealed a pronounced influence of the OSDA on the fluoride dynamics: Whereas samples containing tetrapropylammonium (TPA) exhibit dynamic disorder at RT, the dynamic behaviour is frozen out when using methyltributylammonium (MTBA) as OSDA.[27,28] AIMD simulations revealed that the more heterogeneous charge distribution of MTBA leads to a stronger electrostatic interaction with the fluoride anions, resulting in a larger energetic penalty for a displacement from their initial position and, hence, a reduction of dynamic disorder.[31] In an investigation of AST-type systems, the nature of the OSDA was found to have a significant impact on the ordering of fluoride displacements within the *d4r* cages in $AlPO_4$ and $GaPO_4$ zeotypes.[32] In the view of these earlier findings, some further insights into the systems studied here can be expected from an analysis of the F–OSDA interactions. Assuming that the positive charge of the OSDA is primarily localised in the vicinity of the nitrogen atoms (and the Co atom in $[Co(cp)_2]^+$), an analysis of the F–N/F–Co RDFs can be used to evaluate the role of interactions between the positively polarised part of the OSDA and the fluoride anions.

The F–Co RDF of NON and the F–N RDFs of all other zeolites obtained for 298 K are shown in **Figure 10**. It is apparent that the variety of framework topologies and OSDA molecular structures leads to very different RDFs, with the first maximum being centred at distances ranging from 5.40 Å in CHA to about 7.80 Å in STF, F@Si10. Furthermore, it also clear that there is no correlation between the shortest F–N/F–Co distance and the occurrence of dynamic disorder: For example, the first maximum in the F–N RDF of IFR appears at a lower distance than that in the F–Co RDF of NON. As such, the interaction between OSDA cations and fluoride anions cannot be established as a main factor that determines the distinct dynamic behaviour in the zeolites investigated in this study. Nevertheless, it remains conceivable that a change of the OSDA might reduce or even prevent dynamic disorder, especially if the OSDA has a more heterogeneous charge distribution, as observed previously for MFI.
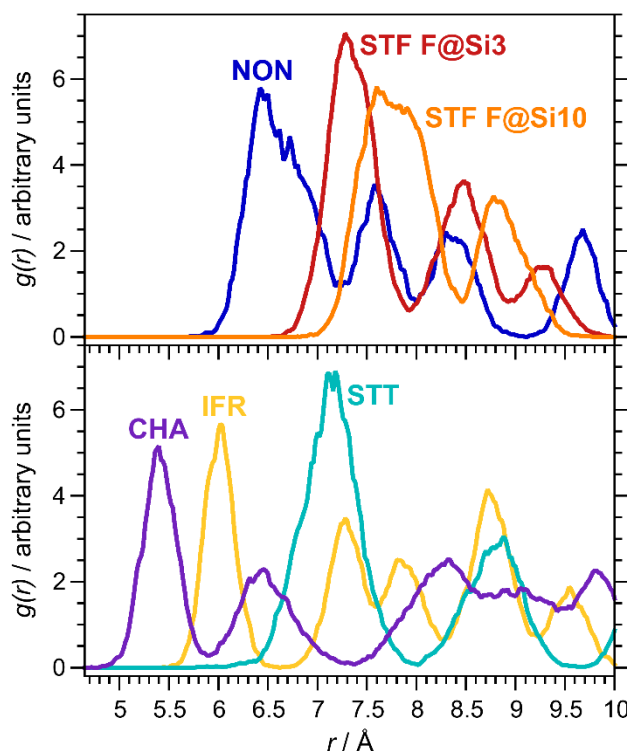

Figure 10: F–Co RDF (NON) and F–N RDFs (other zeolites) obtained from 298 K trajectories.

Additionally, the discrepancy between the pronounced dynamic disorder in IFR and the large value of ΔE_{rel} of the F@Si6_2 site is worth a more detailed analysis. As the two Si atoms have an equivalent environment when only the framework is considered, the large difference in energy must stem from interactions with the OSDA, and the above analysis identified the shorter distance between the fluoride anion and the O atom of the BQol$^+$ OSDA as the reason why F@Si6_2 is

energetically less favourable (**Figure 4**). There are two possible explanations why this large energy difference does not prevent the dynamic motion between the F@Si6_1 and F@Si6_2 sites: Firstly, the thermal motion of the O_{BQol} atoms could lead to an increase of the overall average F–O_{BQol} distance, reducing the energy difference between the two fluoride locations. Alternatively, fluoride anions and O_{BQol} atoms might move in a concerted fashion, so that the hopping of a fluoride anion would coincide with a change of position of the closest O_{BQol} atom. In this context, it is worth noting that the displacement ellipsoid of the O_{BQol} atoms in the experimental structure is large and highly anisotropic, with the longest axis of the displacement lying roughly parallel to the *a* axis (**Figure S18**).[14] This indicates significant thermal oscillations of these atoms, but provides no evidence for a correlation with the dynamic disorder of the fluoride anions, which are displaced along *b* (**Figure 5**). Further evidence for the first of the above hypotheses can be obtained from the AIMD results: The F–O_{BQol} RDF, shown for all three temperatures in **Figure S19** (Supporting Information), exhibits a relatively broad first maximum centred at about 6.3 Å. As becomes clear from the plot of the cumulative $g(r)$, this maximum includes contacts to the nearest and second-nearest O_{BQol} atom. The cumulative $g(r)$ for 298 K reaches a value of 0.5 at a distance of about 5.96 Å. In other words, F–O_{BQol} contacts shorter than this distance occur only during 50% of the total simulation time. Compared to the distances in the DFT-optimised structures (5.80 Å for F@Si6_1, 5.45 Å for F@Si6_2), this is a significant shift towards a larger average F–O_{BQol} separation, which would weaken the electrostatic repulsion and facilitate hopping events between the two F@Si6 positions. The second hypothesis of a concerted hopping can be ruled out by plotting the *y* coordinates of adjacent F and O_{BQol} atoms together. This has been done exemplarily for three F–O_{Bqol} pairs in **Figure S20**. In all three plots, the hopping of fluoride anions is clearly visible as a discontinuous change in *y* coordinate, whereas the O_{BQol} atoms show only random oscillations. It can thus be concluded that the dynamic disorder of the fluoride anions is not coupled to, let alone triggered by, displacements of the closest O_{BQol} atoms.

4 Conclusions

The comparison of DFT optimisation results and experimental structure data has shown that the PBE-D3 calculations deliver a correct prediction of the lowest-energy fluoride location in the majority of cases. This indicates that calculations at this level of theory, which are relatively routinely feasible with state-of-the-art computing resources, can be used to search for likely fluoride locations, either to validate the experimentally determined positions or to predict them in cases where an unambiguous determination from diffraction data is not possible. The combination of diffraction, DFT, and solid-state NMR methods can enable a very comprehensive structural characterisation.[24,51,52] Previous work on MWW- and AST-type zeolites has shown that

the energetic ordering of different configurations is strongly influenced by the presence of the OSDA molecules, which should therefore be included in the calculations.[24,30] As a consequence, the correct localisation of the organic cations in the larger zeolite pores may, in many cases, be the larger challenge. However, if the OSDA cations are correctly placed in the structure model, the present results indicate that there is reason to be confident about the fluoride positions obtained from DFT. In fact, this issue could be, at least partially, responsible for the discrepancies between calculations and experiment observed for STF: Whereas the positions of the non-hydrogen OSDA atoms in NON, IFR, STT, and CHA were determined from single-crystal X-ray diffraction data (in some cases using synchrotron radiation),[11–14,17] the structure of STF-type Mu-26 was refined from powder data.[21] As the DMASD[+] cations could not be localised with Fourier difference methods, presumably due to disorder, their initial positions were obtained using force-field based modelling with the DREIDING force field.[34] While this is, generally, a well-tested procedure,[31,53–55] it cannot be ruled out that the orientation of the OSDA is different in real samples, or that several orientations coexist. Due to the significant impact of framework-OSDA interactions on the equilibrium location of fluoride anions, such an erroneous OSDA orientation could cause an error in the energetic ordering obtained from DFT.

The following factors determining the energetically preferred fluoride location(s) in a system could be identified on the basis of the DFT optimisations:

1) the local environment of the silicon atom, with a strong tendency to favour Si sites that are associated with 4MR faces of the cage;
2) the distribution of $[SiO_4F]^-$ units within the structure, with a tendency to avoid close proximity of such units;
3) interactions with the OSDA. These can be of a variable nature, including attraction/repulsion between fluoride anions and positively/negatively polarised parts of the OSDA, as well as interactions that affect the local geometry around the Si atom (*e.g.*, hydrogen bonds).

Given the multitude of factors at play, and the difficulties in establishing generalisable relationships, it appears that no universal crystal-chemical rules could be devised that would allow for an *a priori* prediction of the most probable fluoride position in a given all-silica zeolite without further input from experiments and/or DFT calculations. Additionally, the analysis of the AIMD results has shown that the inclusion of thermal motion will tend to reduce the energy differences between different sites, in some cases (IFR, CHA) leading to dynamic disorder of fluoride anions over positions having large energy differences ΔE_{rel} according to the static calculations. This aspect should be kept in mind when evaluating the energetic ordering of different fluoride locations.

With regard to the dynamic disorder of fluoride anions, the results of the AIMD simulations agree well with experimental findings. The accurate reproduction of dynamic disorder over three non-equivalent sites in STT is particularly impressive. In the case of STF and CHA, the AIMD results are less clear-cut than for the other three zeolites, indicating that dynamic disorder is absent at RT, but that it should occur at elevated temperatures. The short duration of the simulations puts limitations on this interpretation, and it would be necessary to sample longer simulation times to corroborate this conclusion. Altogether, the results show that DFT-based AIMD simulations are able to make relatively reliable predictions regarding the occurrence or absence of dynamic disorder, at least on a qualitative level. Such calculations could thus find use in materials characterisation, and they might prove particularly valuable in cases where NMR measurements deliver ambiguous results (as is the case for CHA).

Primarily, the differences in the dynamic behaviour of fluoride anions among the zeolites studied can be explained by differences in the local environment: Where relatively short contacts to secondary Si atoms are present, the primary F–Si bond is weakened, and the probability of dynamic "jumps" is increased. In other words, the occurrence/absence of dynamic disorder depends largely on the geometry of the cage in which the fluoride anion resides, whereas interactions with the OSDA cations appear to play only a secondary role. Moreover, the energetic role of framework-OSDA interactions can be expected to decrease with temperature due to the much larger freedom of motion of the OSDA cations in comparison to framework atoms.

The present work has shown that AIMD simulations are a suitable tool to study the intricacies of fluoride dynamic disorder, allowing for predictions of its occurrence as well as an understanding of its origins. Beyond furthering fundamental understanding of these complex host-guest systems, such calculations could be exploited to investigate the structure-directing effects of fluoride anions during zeolite synthesis. Whereas previous predictions of the phase selectivity among different possible zeolite frameworks have largely made use of static DFT calculations (possibly including thermal effects in the framework of the harmonic approximation),[22] the use of AIMD simulations would allow for a direct inclusion of the role of temperature. Differences in the dynamic behaviour of fluoride among different phases might have a subtle, but potentially non-negligible effect on the relative stability and its temperature dependence. In addition to studies of zeolite crystal structures, it could also be interesting to investigate the behaviour of fluoride anions in finite building units (individual cages or assemblies of cages), which could occur as precursors during zeolite formation. Naturally, these potential uses are not restricted to all-silica zeolites, but similar strategies could be applied to all zeolite-like materials that can be synthesised in the presence of fluoride.

Supporting Information

The PDF document supplied as Supporting Information contains the following additional information: Crystal structure figures of zeolite models, further results of DFT optimisations (lattice parameters, relative energies) and AIMD calculations (RMSDs, RDFs, plots of selected average structures). Moreover, an EXCEL file containing analysis results as well as sample input files and calculation results (optimised structures, AIMD trajectories, AIMD average structures) are accessible from: https://doi.org/10.6084/m9.figshare.13603664.v1

References

1   E. M. Flanigen, R. L. Patton, Patent US4073865 A, 1978.

2   J. L. Guth, H. Kessler and R. Wey, *Stud. Surf. Sci. Catal.*, 1986, **28**, 121–128.

3   M. A. Camblor and L. A. Villaescusa, *Top. Catal.*, 1999, **9**, 59–76.

4   P. Caullet, J. Paillaud, A. Simon-Masseron, M. Soulard and J. Patarin, *Comptes Rendus Chim.*, 2005, **8**, 245–266.

5   S. I. Zones, S. Hwang, S. Elomari, I. Ogino, M. E. Davis and A. W. Burton, *Comptes Rendus Chim.*, 2005, **8**, 267–282.

6   M. Moliner, C. Martínez and A. Corma, *Chem. Mater.*, 2014, **26**, 246–258.

7   H. Koller, R. F. Lobo, S. L. Burkett and M. E. Davis, *J. Phys. Chem.*, 1995, **99**, 12588–12596.

8   G. Brunklaus, H. Koller and S. I. Zones, *Angew. Chemie - Int. Ed.*, 2016, **55**, 14459–14463.

9   D. S. Wragg, R. E. Morris and A. W. Burton, *Chem. Mater.*, 2008, **20**, 1561–1570.

10   C. Baerlocher and L. B. McCusker, *http://www.iza-structure.org/databases/*, 2018.

11   G. van de Goor, C. C. Freyhardt and P. Behrens, *Z. Anorg. Allg. Chemie*, 1995, **621**, 311–322.

12   M. A. Camblor, M.-J. Díaz-Cabañas, J. Perez-Pariente, S. J. Teat, W. Clegg, I. J. Shannon, P. Lightfoot, P. A. Wright and R. E. Morris, *Angew. Chemie Int. Ed.*, 1998, **37**, 2122–2126.

13   I. Bull, L. A. Villaescusa, S. J. Teat, M. A. Camblor, P. A. Wright, P. Lightfoot and R. E. Morris, *J. Am. Chem. Soc.*, 2000, **122**, 7128–7129.

14 L. A. Villaescusa, P. S. Wheatley, I. Bull, P. Lightfoot and R. E. Morris, *J. Am. Chem. Soc.*, 2001, **123**, 8797–8805.

15 E. Aubert, F. Porcher, M. Souhassou, V. Petříček and C. Lecomte, *J. Phys. Chem. B*, 2002, **106**, 1110–1117.

16 A. Corma, M. Puche, F. Rey, G. Sankar and S. J. Teat, *Angew. Chemie - Int. Ed.*, 2003, **42**, 1156–1159.

17 L. A. Villaescusa, I. Bull, P. S. Wheatley, P. Lightfoot and R. E. Morris, *J. Mater. Chem.*, 2003, **13**, 1978–1982.

18 R. J. Darton, D. H. Brouwer, C. A. Fyfe, L. A. Villaescusa and R. E. Morris, *Chem. Mater.*, 2004, **16**, 600–603.

19 M. Arranz, J. Pérez-Pariente, P. A. Wright, A. M. Z. Slawin, T. Blasco, L. Gómez-Hortigüela and F. Cora, *Chem. Mater.*, 2005, **17**, 4374–4385.

20 S. I. Zones, R. J. Darton, R. Morris and S.-J. Hwang, *J. Phys. Chem. B*, 2005, **109**, 652–661.

21 J. Paillaud, B. Harbuzaru and J. Patarin, *Microporous Mesoporous Mater.*, 2007, **105**, 89–100.

22 C. M. Zicovich-Wilson, F. Gándara, A. Monge and M. A. Camblor, *J. Am. Chem. Soc.*, 2010, **132**, 3461–3471.

23 A. Pulido, A. Corma and G. Sastre, *J. Phys. Chem. B*, 2006, **110**, 23951–23961.

24 P. Lu, L. Gómez-Hortigüela and M. A. Camblor, *Chem. - A Eur. J.*, 2019, **25**, 1561–1572.

25 H. Koller, A. Wölker, H. Eckert, C. Panz and P. Behrens, *Angew. Chemie Int. Ed.*, 1997, **36**, 2823–2825.

26 H. Koller, A. Wölker, L. A. Villaescusa, M. J. Diaz-Cabañas, S. Valencia and M. A. Camblor, *J. Am. Chem. Soc.*, 1999, **121**, 3368–3376.

27 S. L. Brace, P. Wormald and R. J. Darton, *Phys. Chem. Chem. Phys.*, 2015, **17**, 11950–11953.

28 S. Brace, Synthetic and structural studies of high silica MFI zeolites, PhD thesis, Keele University, 2017 (https://eprints.keele.ac.uk/3778/).

29 C. A. Fyfe, D. H. Brouwer, A. R. Lewis, L. A. Villaescusa and R. E. Morris, *J. Am. Chem. Soc.*, 2002, **124**, 7770–7778.

30 M. Fischer, *J. Phys. Chem. C*, 2019, **123**, 1852–1865.

31 M. Fischer, *J. Phys. Chem. C*, 2020, **124**, 5690–5701.

32 M. Fischer and L. Freymann, *ChemPhysChem*, 2021, **22**, 40–54.

33 D. S. BIOVIA, *BIOVIA Materials Studio 2019*, DS Biovia, 2019.

34 S. L. Mayo, B. D. Olafson and W. A. Goddard, *J. Phys. Chem.*, 1990, **94**, 8897–8909.

35 T. D. Kühne, M. Iannuzzi, M. Del Ben, V. V. Rybkin, P. Seewald, F. Stein, T. Laino, R. Z. Khaliullin, O. Schütt, F. Schiffmann, D. Golze, J. Wilhelm, S. Chulkov, M. H. Bani-Hashemian, V. Weber, U. Borštnik, M. Taillefumier, A. S. Jakobovits, A. Lazzaro, H. Pabst, T. Müller, R. Schade, M. Guidon, S. Andermatt, N. Holmberg, G. K. Schenter, A. Hehn, A. Bussy, F. Belleflamme, G. Tabacchi, A. Glöß, M. Lass, I. Bethune, C. J. Mundy, C. Plessl, M. Watkins, J. VandeVondele, M. Krack and J. Hutter, *J. Chem. Phys.*, 2020, **152**, 194103.

36 J. P. Perdew, K. Burke and M. Ernzerhof, *Phys. Rev. Lett.*, 1996, **77**, 3865–3868.

37 S. Grimme, J. Antony, S. Ehrlich and H. Krieg, *J. Chem. Phys.*, 2010, **132**, 154104.

38 M. Krack, *Theor. Chem. Acc.*, 2005, **114**, 145–152.

39 J. VandeVondele and J. Hutter, *J. Chem. Phys.*, 2007, **127**, 114105.

40 S. Nosé, *J. Chem. Phys.*, 1984, **81**, 511–519.

41 W. G. Hoover, *Phys. Rev. A*, 1985, **31**, 1695–1697.

42 W. Humphrey, A. Dalke and K. Schulten, *J. Mol. Graph.*, 1996, **14**, 33–38.

43 K. Momma and F. Izumi, *J. Appl. Crystallogr.*, 2011, **44**, 1272–1276.

44 T. Hahn (Ed.), *International Tables for Crystallography Vol. A*, International Union of Crystallography, Chester, England, 2006.

45 S. I. Zones, A. W. Burton, G. S. Lee and M. M. Olmstead, *J. Am. Chem. Soc.*, 2007, **129**, 9066–9079.

46 L. S. Dent and J. V. Smith, *Nature*, 1958, **181**, 1794–1796.

47 M.-J. Díaz-Cabañas, P. A. Barrett and M. A. Camblor, *Chem. Commun.*, 1998, 1881–1882.

48 F. L. Hirshfeld, *Theor. Chim. Acta*, 1977, **44**, 129–138.

49 M. Fischer, W. J. Kim, M. Badawi and S. Lebègue, *J. Chem. Phys.*, 2019, **150**, 094102.

50 M. P. Attfield, C. R. A. Catlow and A. A. Sokol, *Chem. Mater.*, 2001, **13**, 4708–4713.

51 R. T. Rigo, S. R. G. Balestra, S. Hamad, R. Bueno-Perez, A. R. Ruiz-Salvador, S. Calero and M. A. Camblor, *J. Mater. Chem. A*, 2018, **6**, 15110–15122.

52 J. Holzinger, M. Nielsen, P. Beato, R. Y. Brogaard, C. Buono, M. Dyballa, H. Falsig, J. Skibsted and S. Svelle, *J. Phys. Chem. C*, 2019, **123**, 7831–7844.

53 R. Pophale, F. Daeyaert and M. W. Deem, *J. Mater. Chem. A*, 2013, **1**, 6750–6760.

54 J. E. Schmidt, M. W. Deem, C. Lew and T. M. Davis, *Top. Catal.*, 2015, **58**, 410–415.

55 F. Daeyaert and M. W. Deem, *ChemPlusChem*, 2020, **85**, 277–284.